Supplemental results

Weighted gene correlation network analysis reveals loss of preservation and connectivity of glial and immune modules

We clustered the bulk RNAseq samples as a preliminary analysis to uncover the main factors that drive gene variation in our dataset. Clustering of the samples based on a distance metric calculated from normalized gene expression identified 6 clusters, some with predominance of cortical samples (Cl3 and Cl5), striatal samples (Cl2, Cl4, Cl6), control samples (Cl3-4), or HD samples (Cl2 and Cl6 – **Figure S1B**). Clusters Cl2 and Cl4 were enriched in samples from females and males, respectively. These results show a strong influence of brain region and condition on gene expression, as expected.

To understand patterns of gene co-regulation and dysregulation in HD brain regions, we performed weighted gene correlation network analysis (WGCNA) on control and HD bulk RNAseq samples. Networks from control and HD samples were constructed separately to examine the changes in the patterns of gene correlation in HD (**Figure S2A**) as described in the Methods. Gene-module memberships are provided in Supplementary Table 3. 22 and 20 modules were identified in the control and HD networks, respectively (**Figure S2A**). Multiple control modules exhibited gene overlap with HD modules, however, some HD gene modules showed minimal overlap with control modules. For instance, the HD purple and turquoise modules only significantly overlapped with the control grey (background) module (**Figure S2B**) - suggesting that some genes in HD gain correlation. We next correlated the genes in the control and HD modules to anatomic region, sex, age, and CAG repeat length (in HD modules) and found that there were several control modules with significant, strong, positive and negative correlations with anatomic regions (**Figure S2C**), and CAG repeat length (in HD modules). In particular, the HD purple module (which did not exhibit significant overlap with control modules) and the lightgreen module were significantly positively correlated with CAG repeat length, and the black, blue, turquoise, and lightcyan were significantly negatively correlated with CAG repeat lengths. The royalblue and turquoise showed no significant trait correlations (**Figure S2C**), which suggests they correspond to regional-agnostic gene programs.

Examination of preservation statistics reveals that several modules showed minimal preservation overall, and in particular, loss of density and connectivity (**Figure S2D** and **Supplementary Table-3**). The loss of connectivity of select modules is shown in **Figure S2G**. These modules include the lightgreen, darkred, pink, tan, lightyellow, and royalblue. The lightgreen and royalblue modules were positively correlated with the caudate region, whereas the darkred, pink and tan modules were negatively correlated. In fact, the darkered displayed a correlation with the cingulate region, and the tan module showed correlations with cingulate and accumbens regions. Examination of gene ontologies enriched in the module genes of the most poorly preserved modules

incriminate splicing, DNA repair, mitosis, transcription, nuclear export, metabolism, response to iron ions, and dopamine metabolism (**Figure S2E** and **Supplementary Table-3**). Next, we examined the GO terms that are enriched in the HD modules that were significantly positively correlated with CAG repeat length – including the lightgreen and purple. The results incriminate enrichment of genes involved in immune response, T cell function, translation, proteosomal function, polyubiquitination, glial function, and response to stress. Of the genes enriched in the modules negatively correlated with CAG repeat length, our results showed enrichment of genes involved with vascular function and angiogenesis (lightcyan), DNA related ontologies like base-excision repair and methylation (blue), immune-related ontologies like regulation of T-cell activation (midnight blue), and response to unfolded protein, RNA splicing, cell aging, and myeloid cell homeostasis (black - **Figure S2F** and **Supplementary Table-3**). Given the involvement of immune genes in modules poorly preserved in HD, we asked if modules associated with immune (T-cell/microglial) and astroglial module genes display altered connectivity. We focused on the control modules with interesting microglial (*TSPO*) and astrocytic (*HEPACAM*) hubs - the black and brown, respectively (**Supplementary table-3**). Similar to poorly preserved modules (lightgreen, lightcyan, darkred, tan, pink), hub genes in the control black (immune) and brown (astroglial/immune) modules showed loss of connectivity of the hub genes, which appear to be members of other modules in the HD network (**Figure S2G**). Together, these results confirm that HD indeed significantly influences astrocyte and microglial gene expression.

Astrocytes in the caudate nucleus appear dysmorphic

The morphology of astrocytes immune-stained with GFAP appeared different compared with controls. HD astrocytes were dysmorphic with reduced process length. To quantify this phenotype, we measured the average process length of GFAP+ astrocytes in the caudate from three HD and three controls. The results showed a reduction in average process length in HD (**Figure S4C**).

Abundance Analysis in Astrocytes

In order to evaluate whether astrocytic clusters were enriched or depleted in HD, we conducted differential abundance analysis. As can be seen in **Figure S5F**, cluster F2 was enriched in HD. Differential abundance analysis confirmed that this cluster was particularly enriched in HD in the accumbens (logFC 1.49, p value 0.00082), and a similar pattern was seen in the cingulate, though lacking significance (logFC 0.474, p value 0.2105). This further supports our data suggesting that cluster F2 is enriched in HD in the accumbens (**Table S5**). When examining cluster F1 which showed enrichment of the neuroprotective geneset (**Figure 4B**), the differential abundance results showed that it was enriched in the cingulate cortex (**Figure S5G**). However, we did not find significant differences in F1 abundance between HD and controls (**Table S5**).

Differentially expressed genes in neurons

We performed differential gene expression analysis on major neuronal cell types detected in the striatal and cortical regions of our study. Volcano plots displaying top DEGs for each cell type in all three brain regions are displayed in **Figure S7A-C**. The differential gene expression analysis of neurons revealed that the overall numbers of DEGs were significantly larger in the striatal region than the cortex (**Figure S7D**). We saw some of the highest numbers of DEGs in the SPN cells with the accumbens dSPN having the largest number of DEGs decreased and the highest upregulation coming from the caudate dSPN. In the cingulate cortex, the glutamatergic neurons had significantly more DEGs compared to the GABAergic neurons and the number of DEGs from the GABAergic neurons were significantly lower compared to the striatal regions. The DEGs are provided in **Supplementary Table 8**.

Further examination of the DEGs showed the expected decrements of PCP4 and PDE10A in all SPNs in the caudate and accumbens (**Supplementary Table-8**). In dSPNs of both regions, we found the expression of *PENK* to be increased. Changes in these genes have been documented by multiple studies [1-3]. Moreover, the caudate dSPN showed a significant decrease in the expression of TAC1, but this was not found to be significant in the accumbens. Among the set of genes that were shared and downregulated between SPNs across the two regions were *MALAT1*, *FTX*, *RBFOX1*, *RYR3*, and *RYR2*. Interestingly, we observed that the expression of *CLU* to be increased in dSPN and iSPN neurons in the accumbens and caudate along with a significant increase in accumbens GABAergic cells as well.

We compared our DEG results from the caudate to Lee et al.[4] SPN DEG. We found 291 genes in common among dSPN in the caudate that were upregulated in our analysis and 251 genes that were downregulated (**Supplementary Table 8**). Many of the genes that were upregulated were involved in heat shock protein response. More specifically, these genes included *HSB1, HSPA4, HSPA8, HSPA1A*, and *CLU*. Genes that were downregulated in dSPN included *SLC24A2, RYR3, CACNA1A, JPH4*, and *CALM1* which are known to be involved in calcium ion activity. Comparing the iSPN neurons to the Lee et al. findings revealed there were 210 shared genes that were upregulated and 327 shared genes that were downregulated. Many of the shared genes that were upregulated were similar to the dSPN like *HSPA1A, CLU,* and *DNAJA1*. Among the upregulated genes, a large portion of it were involved in binding to unfolded proteins. In addition, we examined the medium spiny neuron DEG from Malaiya et al[4] and confirmed that many of the genes reported to be downregulated across all SPN subtypes were indeed downregulated in dSPN and iSPN in the striatal brain regions of our data too. These genes include *PDE10A, PDE1B, ADCY5, ATP2B1,* and *ARRP21*. Shared upregulated genes in the iSPN are largely involved in response to unfolded protein which are driven by heat shock protein genes. On the other hand, some shared downregulated genes in the iSPN were involved with disruption of ion channel activity as driven by the decreased expression of genes like GRIN2A, GRIA1, GRIN2B, NLGN1, DAPK1, DLG1, and DLG2.

We also compared our GO terms to Lee et al. and found that our results are consistent with the decrease of phosphatidylinositol signaling system in accumbens dSPN and iSPN as well as in the caudate dSPN but not caudate iSPN. MAPK signaling was only found to be increased among accumbens dSPN. Conversely, the GO term cholinergic synapse was increased in Lee et al. but decreased in all of our SPN in accumbens and caudate. Spliceosome activity also was decreased as expected among all SPN in all regions. These differences may arise from differences in the regions analyzed in Lee et al, which included the putamen – a region not included in our analysis. In addition to these comparisons, we also report genes involved in various ion channel activity as well as lipid phosphorylation to be depleted in all SPN in both the accumbens and caudate (**Figure S7E**). There were differences and similarities between the caudate and accumbens SPNs, and between iSPNs and dSPNs. For example, dendrite morphogenesis GO was increased in accumbens SPN but decreased in the caudate, while glutamatergic receptor activity GO term was significantly enriched in decreased genes in both groups and both regions. Conversely, the GO lipoprotein particle receptor binding was only enriched in increased DEGs in the accumbens dSPNs. Also, GABA neurons showed fewer DEGs than other neuronal types, and even these were regionally diverse, being mildest in the cingulate cortex (**Figure S7D**). Among the cingulate neurons, we observe a general decrease in genes related to metabolism in the glutamatergic and GABAergic neurons.

Other astrocytic proteins

Next, we turned our attention to other markers of the putative neuroprotective protoplasmic clusters P1 and P3 (**Figure 4D**). *CLU* was expressed in both clusters and thus quantified it in the cingulate cortex and caudate nucleus. Quantification of CLU by immunostaining showed that it was decreased in the cingulate but not in the caudate HD astrocytes (**Figure S8A-D**). Overall, these results show that even within the same cluster, astrocytes can show different patterns of protein expression. Thus, putative neuroprotective astrocytes in the cingulate are different from those in the caudate nucleus; they increase metallothioneins and decrease CLU, while caudate astrocytes of the same cluster did not exhibit altered expression of CLU, and even showed decreased levels of MT3.

We asked if CLU overexpression alters expression levels of metallothioneins (**Figure S9B-C**). In CLU-overexpressing astrocytes there was a modest upregulation of CLU, but no increase in metallothionein 1 genes (**Figure S9B-C**). Additional studies are needed to elaborate on the relationship between CLU and MT's in astrocytes.

Astrocyte-Microglia crosstalk in HD

Given the known crosstalk between astrocytes and microglia[5], we asked if microglial gene expression is altered in HD brains. Notwithstanding the limitations of snRNAseq in analyzing microglial cells[6], and the relative paucity of retrieved cells, we performed analysis on HD and control myeloid cells in our cohort. We first subclustered our myeloid cells from the three brain regions analyzed. We discovered 3 major clusters which corresponded to microglial cells, blood-derived myeloid cells (monocyte-derived

macrophages), and T-cells (**Figure S10A**). This is further illustrated by examining gene marker expression, which shows *SORL1* and *DOCK4* in microglia, *CD163* in monocyte-like cells, and *CD96* as well as *THEMIS* in T-cells (**Figure S10B** and **Supplementary Table-9**). Since the number of macrophages and T-cells were considerably than microglial cells (**Supplementary Table-9**), we decided to focus on the latter for downstream analysis. Microglial cells were distributed across all brain regions examined, unlike T-cells and macrophages, which we mainly retrieved from HD striatal samples (**Supplementary Table-9**). To understand how the microglia differ across the three brain regions in HD, we performed DEG analysis in each of the regions (**Figure S10C-E**). Interestingly, heat shock protein gene expression varied between the three brain regions in microglia. For example, *HSPH1* was increased in the accumbens and cingulate but downregulated in the caudate. In addition, several genes were downregulated in the caudate, like *HSPA1A, HSPA1B,* and *HSP90AA1*. Examining the GO enriched in microglial DEGs showed regional differences in microglial responses to HD (**Figure S10F**). As expected, cingulate and accumbens HD microglia upregulated genes involved in heat shock and stress response, but this was not the case in the caudate. Likewise, in the cingulate and accumbens, HD microglia upregulated genes associated with cell scavenger receptors, which are associated with the innate immune response and phagocytosis[7].

Given the heterogeneity of gene expression changes in microglia in HD, and in light of our previous results on astrocyte phenotypic heterogeneity across brain regions in HD, we asked if region-enriched astrocytic phenotypes altered microglial function. Specifically, we examined if the neuroprotective astrocytic phenotype, with increased *MT3* expression, led to changes in microglial function. To address that question, we performed co-culture assays between microglia and astrocytes in a trans-well assay, and quantified gene expression in microglia using RNAseq or phagocytosis of fluorescent beads using FACS (**Figure S11A**). We overexpressed *MT3* and *CLU* (which were both markers of neuroprotective protoplasmic clusters 1 and 3), or GFP in astrocytes, and co-cultured with control microglia. We were interested in CLU because we previously reported that CLU was increased in astrocytes in the context of glioma microenvironment, and that CLU+ astrocytes can alter gene expression of glioma cells in a manner that reduced expression of immune-related genes[8]. This experimental design allowed us to measure how changes in astrocyte phenotype influence microglial function via factors secreted into the media by astrocytes. Our results showed that co-culture of astrocytes with microglia significantly altered gene expression in microglia (**Figure S11B** – see PCA, and **Supplementary Table-9**). However, while MT3 overexpression significantly altered gene expression in microglia (**Figure S11D**), that was not the case in microglia co-cultured with CLU overexpressing astrocytes (**Figure S11C**). GO enrichment analysis showed that MT3-astrocytes caused microglia to upregulate genes associated with lipid and fatty acid metabolism and transport (**Figure S11E**). That stated, we did not identify changes in pathways related to phagocytosis.

Given that microglial gene expression can be altered by MT3-astrocytes, we asked if the genes significantly increased or decreased in microglia *in vitro* by MT3 astrocytes (referred as MT3 DEG up and MT3 DEG down signatures) were enriched in the DEGs in HD vs control microglia (cluster 0) from our snRNAseq data across the three brain regions. We also measured the enrichment of genes positively and negatively correlated with CAG repeat length, because CAG-correlated genes were enriched in pathways related to immune functions (main text - **Figure 1F**). Moreover, we measured the enrichment of the GO term phagocytosis in the region-specific microglial DEGs because phagocytosis is a general signature for which functional assays are available to us (**Figure S11F).** We found that while the *in vitro* MT3 DEG up signature was significantly enriched in the snRNAseq microglial DEGs in cingulate and approached significance in the nucleus accumbens, the signature was not enriched in the caudate (**Figure S11F**). This finding was consistent with the fact that MTs were significantly increased in the cingulate and accumbens protoplasmic astrocytes (by snRNAseq and IHC validation for cingulate, snRNAseq for accumbens), but not in caudate astrocytes (by snRNASeq and IHC). Also, the term for phagocytosis was not enriched in the microglial DEGs – only in Cluster 0 (microglial cells) marker genes. In addition, genes positively correlated with CAG repeat length were enriched in accumbens microglial DEGs but not other regions. Together, these findings suggest that in addition to the neuroprotective and astroprotective roles of MTs, these proteins may alter microglial gene expression and functional attributes, and these effects may be region-specific.

Functionally, microglia co-cultured with MT3 but not CLU overexpressing astrocytes increased their phagocytic activity (**Figure S11G**). Of note, there is a discrepancy between increased phagocytosis quantified by FACS and the absence of accompanying gene expression changes in phagocytosis-related pathways. This may be explained by the fact that the percentage of microglial cells with increased phagocytosis was relatively low in our assay, thus, gene expression changes may not have been large enough to be detected by bulk RNAseq. It is also possible that the changes in phagocytosis induced by MT3 astrocytes occur on the protein level without durable gene expression changes in phagocytosis-related pathways. It remains to be determined, however, whether increased microglial phagocytic activity is compensatory or deleterious in HD. Additional studies are needed to define the potential functional effects of changes in phagocytosis and lipid metabolism in HD microglia.

Figure S1. Bulk RNAseq samples and CAG repeats. Related to Figure 1. **A**) t-distributed stochastic neighbor (tSNE) embedding of bulk RNAseq samples used in the study color-coded by sex (top), and sequencing batch (bottom) – showing adequate correction for batch- and sex- related effects. **B**) Sample distance heatmap showing the Manhattan distance clustered using the Ward D2 method. Normalized batch corrected counts were used to generate the sample distance. The colored bars on the left indicate the sample clusters, anatomic region (Acc: Accumbens. Caud: Caudate, Cing: Cingulate), and HD grade/Condition (Control (Con) versus HD grades 1-4 & J: juvenile onset HD). **C**) Differences in CAG Repeat length modal peaks measured in the specified brain regions or blood/cerebellum. Barplots of the difference in CAG repeats in each brain region (purple for accumbens, green for caudate, yellow for cingulate) compared to the blood/cerebellum. The x axis values represent the delta change compared to the blood/cerebellum. Positive values indicate higher values in the brain regions specified, and 0 indicates no change. The y axis shows the number of samples which are represented by the x axis value.

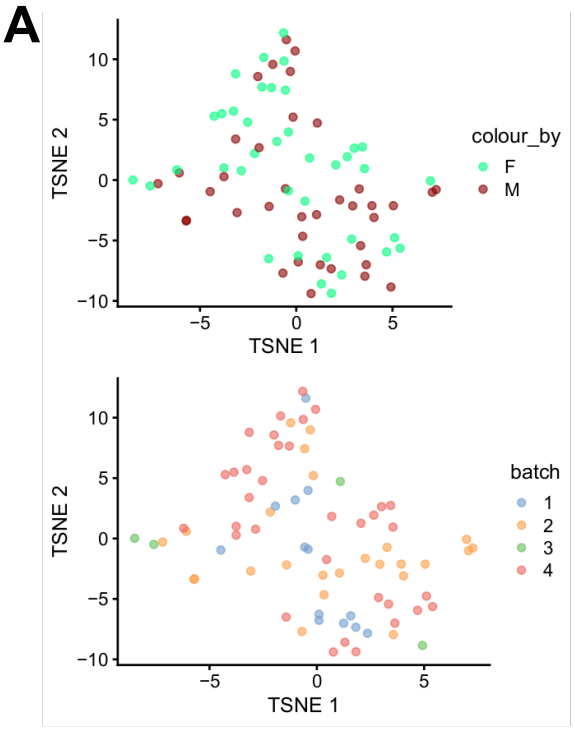
A
TSNE 2
TSNE 1
colour_by
F
M
batch
1
2
3
4

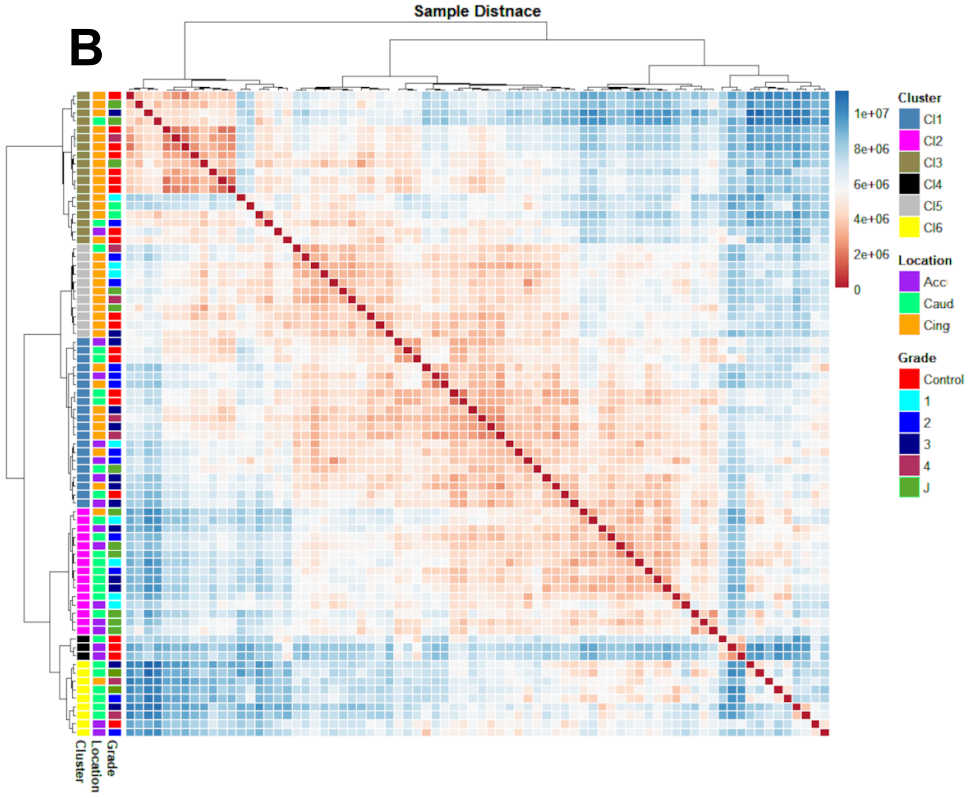
B
Sample Distnace
Cluster
Cl1
Cl2
Cl3
Cl4
Cl5
Cl6
Location
Acc
Caud
Cing
Grade
Control
1
2
3
4
J

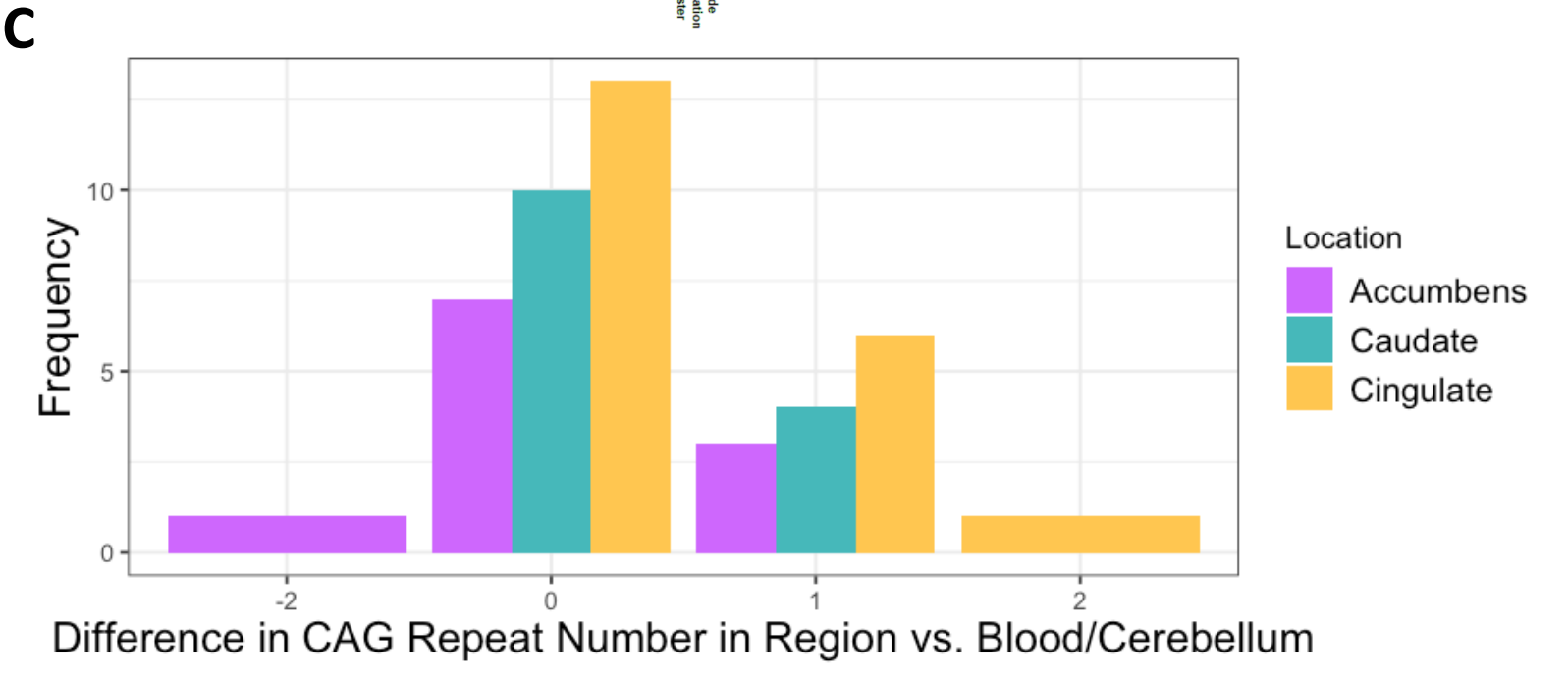
C
Frequency
Difference in CAG Repeat Number in Region vs. Blood/Cerebellum
Location
Accumbens
Caudate
Cingulate

Figure S2. Weighted gene correlation analysis (WGCNA) identifies gene modules that lose preservation in HD. **A**) Dendrograms showing genes clustered hierarchically for control (right) and HD (left) samples. The genes are colored by control or HD network module designations in the colored bars (bottom) as specified, for control (left) and HD (right) dendrograms. **B**) Heatmap showing the overlap between genes in control modules (rows) and HD modules (columns). The number of overlapping genes and p values are indicated in the tiles. **C**) Heatmap of trait-module correlations for the Control (left) and HD (right) network modules. The correlation coefficients and p values in parenthesis are indicated. The module-trait relationships were determined in control and HD expression matrices, separately. **D**) Control module preservation statistics with module size (x-axis) plotted against several module density and connectivity statistics (y-axis). The top row shows the most frequently used summary statistics. The color of the nodes represents gene module membership in the control modules. **E-F**) Gene Ontology (GO) term enrichment analysis showing the top biological process GO terms enriched in the genes of select control (**E**) and HD (**F**) modules. The heatmap shows GO terms as rows, and module names as columns. The negative log10 of the enrichment p value is represented by color. **G**) Subnetwork analysis of the top 25 genes with highest connectivity (hub genes) in the control modules shown in the control subnetwork (left) versus the HD subnetwork (right). Nodes represent genes and edges correlations. The edges with weights less than the mean weight for each subnetwork were trimmed. The size of the circles (gene) represents the hub score as detected in igraph package. The node color in the HD column (right) indicate the module membership of the respective gene in the HD network.

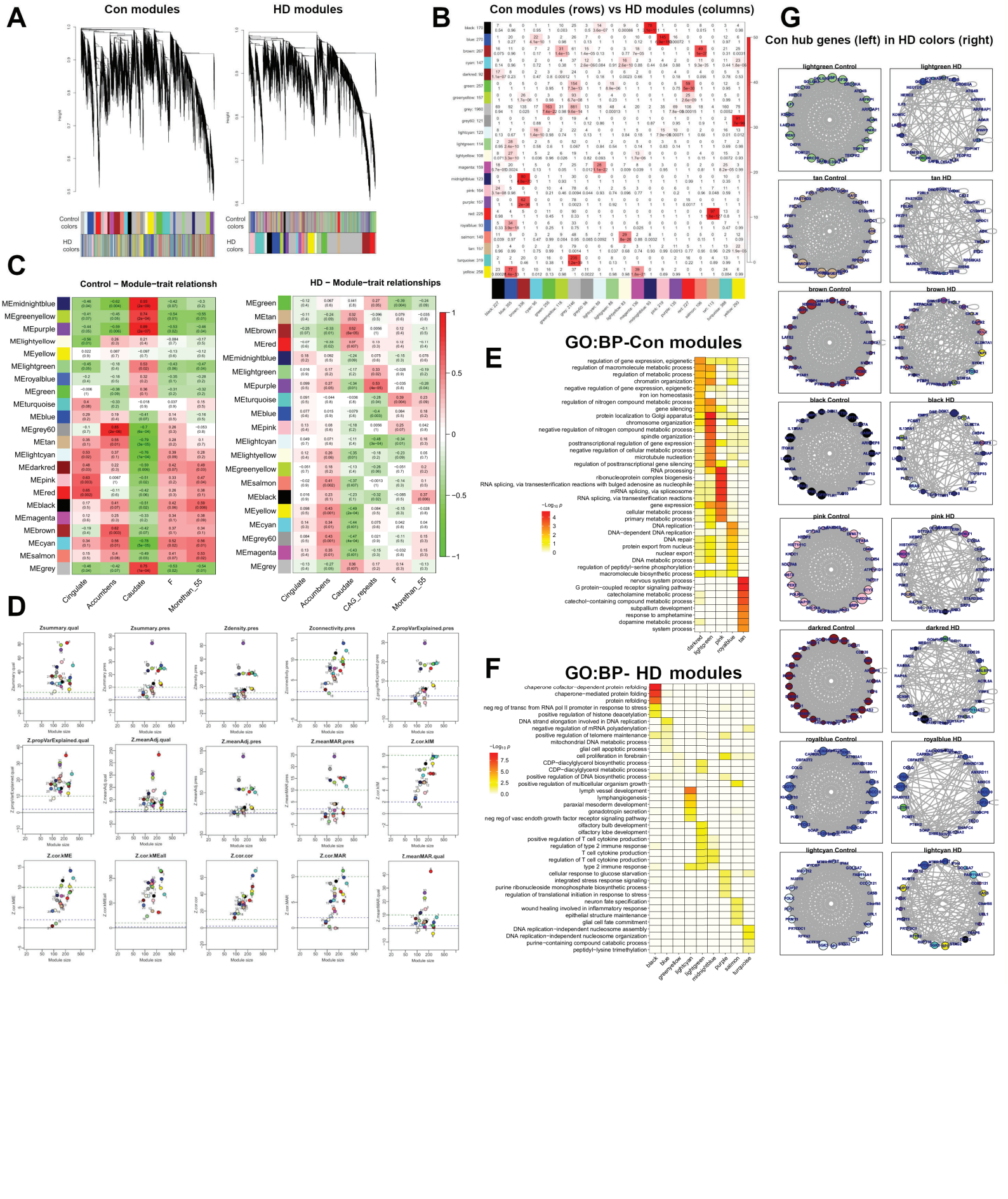
A
Con modules
HD modules
Height
Control colors
HD colors
B
Con modules (rows) vs HD modules (columns)
black: 170
blue: 270
brown: 267
cyan: 147
darkred: 92
green: 257
greenyellow: 157
grey: 1960
grey60: 121
lightcyan: 123
lightgreen: 114
lightyellow: 108
magenta: 159
midnightblue: 123
pink: 164
purple: 157
red: 225
royalblue: 93
salmon: 149
tan: 157
turquoise: 319
yellow: 258
black: 222
blue: 355
brown: 336
cyan: 95
green: 255
greenyellow: 115
grey: 1746
grey60: 88
lightcyan: 89
lightgreen: 85
lightyellow: 85
magenta: 139
midnightblue: 93
pink: 219
purple: 135
red: 227
salmon: 106
tan: 113
turquoise: 368
yellow: 260
C
Control − Module−trait relationsh
HD − Module−trait relationships
MEmidnightblue
MEgreenyellow
MEpurple
MElightyellow
MEyellow
MElightgreen
MEroyalblue
MEgreen
MEturquoise
MEblue
MEgrey60
MEtan
MElightcyan
MEdarkred
MEpink
MEred
MEblack
MEmagenta
MEbrown
MEcyan
MEsalmon
MEgrey
MEgreen
MEtan
MEbrown
MEred
MEmidnightblue
MElightgreen
MEpurple
MEturquoise
MEblue
MEpink
MElightcyan
MElightyellow
MEgreenyellow
MEsalmon
MEblack
MEyellow
MEcyan
MEgrey60
MEmagenta
MEgrey
Cingulate
Accumbens
Caudate
F
Moreithan_55
CAG_repeats
D
Zsummary.qual
Zsummary.pres
Zdensity.pres
Zconnectivity.pres
Z.propVarExplained.pres
Z.propVarExplained.qual
Z.meanAdj.qual
Z.meanAdj.pres
Z.meanMAR.pres
Z.cor.kIM
Z.cor.kME
Z.cor.kMEall
Z.cor.cor
Z.cor.MAR
Z.meanMAR.qual
Module size
E
GO:BP-Con modules
regulation of gene expression, epigenetic
regulation of macromolecule metabolic process
regulation of metabolic process
chromatin organization
negative regulation of gene expression, epigenetic
iron ion homeostasis
regulation of nitrogen compound metabolic process
gene silencing
protein localization to Golgi apparatus
chromosome organization
negative regulation of nitrogen compound metabolic process
spindle organization
posttranscriptional regulation of gene expression
negative regulation of cellular metabolic process
microtubule nucleation
regulation of posttranscriptional gene silencing
RNA processing
ribonucleoprotein complex biogenesis
RNA splicing, via transesterification reactions with bulged adenosine as nucleophile
mRNA splicing, via spliceosome
RNA splicing, via transesterification reactions
gene expression
cellular metabolic process
primary metabolic process
DNA replication
DNA−dependent DNA replication
DNA repair
protein export from nucleus
nuclear export
DNA metabolic process
regulation of peptidyl−serine phosphorylation
macromolecule biosynthetic process
nervous system process
G protein−coupled receptor signaling pathway
catecholamine metabolic process
catecholcontaining compound metabolic process
subpallium development
response to amphetamine
dopamine metabolic process
system process
−Log10 p
darkred
lightgreen
pink
royalblue
tan
F
GO:BP- HD modules
chaperone cofactor−dependent protein refolding
chaperone−mediated protein folding
protein refolding
neg reg of transc from RNA pol II promoter in response to stress
positive regulation of histone deacetylation
DNA strand elongation involved in DNA replication
negative regulation of mRNA polyadenylation
positive regulation of telomere maintenance
mitochondrial DNA metabolic process
glial cell apoptotic process
cell proliferation in forebrain
CDP−diacylglycerol biosynthetic process
CDP−diacylglycerol metabolic process
positive regulation of DNA biosynthetic process
positive regulation of multicellular organism growth
lymph vessel development
lymphangiogenesis
paraxial mesoderm development
gonadotropin secretion
neg reg of vasc endoth growth factor receptor signaling pathway
olfactory bulb development
olfactory lobe development
positive regulation of T cell cytokine production
regulation of type 2 immune response
T cell cytokine production
regulation of T cell cytokine production
type 2 immune response
cellular response to glucose starvation
integrated stress response signaling
glial cell fate commitment
purine ribonucleoside monophosphate biosynthetic process
regulation of translational initiation in response to stress
neuron fate specification
wound healing involved in inflammatory response
epithelial structure maintenance
DNA replication−independent nucleosome assembly
DNA replication−independent nucleosome organization
purine−containing compound catabolic process
peptidyl−lysine trimethylation
−Log10 p
black
blue
greenyellow
lightcyan
lightgreen
midnightblue
purple
salmon
turquoise
G
Con hub genes (left) in HD colors (right)
lightgreen Control
lightgreen HD
tan Control
tan HD
brown Control
brown HD
black Control
black HD
pink Control
pink HD
darkred Control
darkred HD
royalblue Control
royalblue HD
lightcyan Control
lightcyan HD

Figure S3. Lipidomic analysis of HD brains. Related to Figure 2. A) Boxplots of relative abundance of select long-chain lipid species with significant one-way ANOVA p-values for grade. The data is presented with grade (color-coded) on the x-axis. The p-values for Tuckey post-hoc comparisons are indicated in the table (down). Stars indicate significant post-hoc analysis p-values. P values are indicated in the table below figure. The boxplots indicate the median and Q1-3 interquartile range. Whiskers extend to the lowest and highest values from the first and third quartiles, respectively, up to 1.5 times the interquartile range in either direction. Outliers are denoted by points. **B**) Receiver Operating Characteristic (ROC) curve showing the sensitivity (y-axis) and 100-specificity (x-axis) of the sPLS-DA model in distinguishing condition (grade) based on the first 4 components. ROC traces for each grade are represented separately and denoted using the colors indicated on the right. **C**) Scatter plots showing projection of lipidomics samples and integrated lipidomic/RNAseq in the first two latent variables of sPLS. The variance explained by each component is indicated on the axes. The samples are color- and shape- coded by sex. **D**) Correlation network analysis showing the correlation (encoded by edges, with color corresponding to correlation values) between genes and lipid species (nodes). Only the most highly (positively and significantly) correlated nodes are shown. The color of the edges represent the correlation value.

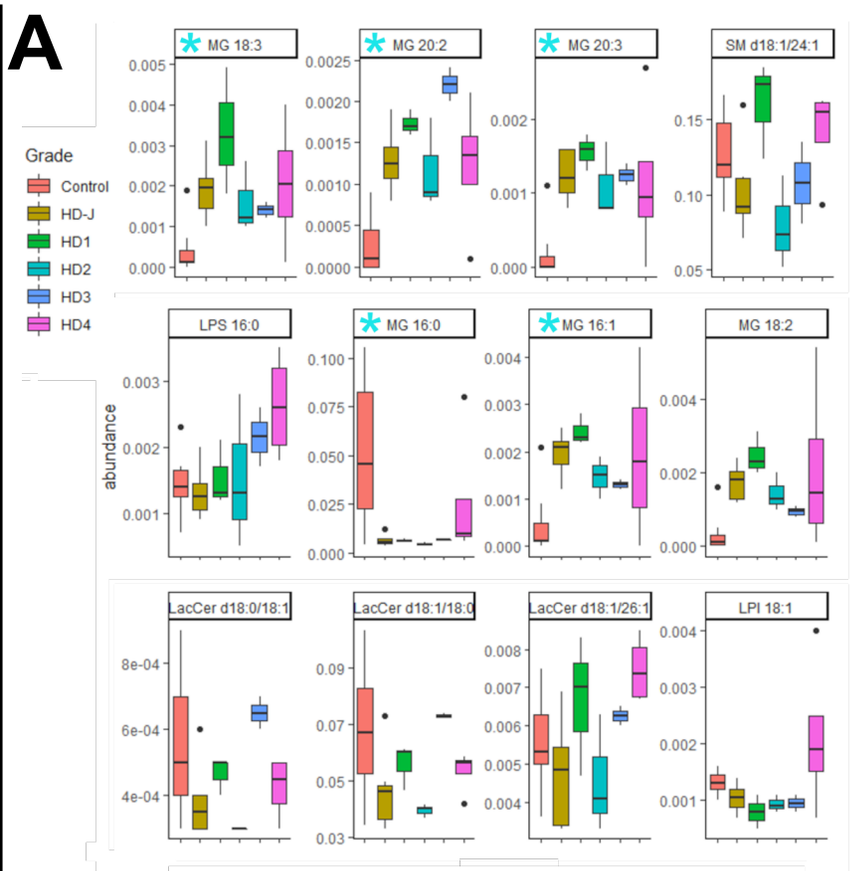

lipid	HDJ.Control	HD1.Control	HD2.Control	HD3.Control	HD4.Control
MG 16:0	**0.0210008**	0.1292716	0.1052063	0.2544323	0.5765550
MG 16:1	**0.0305467**	**0.0350648**	0.5703944	0.8382855	0.1108342
MG 18:2	0.1199753	0.0597440	0.6305894	0.9731304	0.1023397
MG 18:3	**0.0859118**	**0.0052513**	0.5502678	0.8277141	0.1460213
MG 20:2	**0.0047812**	**0.0022329**	0.1023767	**0.0005450**	**0.0388220**
MG 20:3	**0.0140766**	**0.0171300**	0.2050507	0.2016551	0.1014069
SM d18:1/24:1	0.5345822	0.6133371	0.2121135	0.9569118	0.9765289
LacCer d18:0/18:1	0.1645990	0.9322298	0.1256621	0.9589568	0.6641103
LacCer d18:1/18:0	0.1063144	0.8637547	0.1262642	0.9980850	0.6741425
LacCer d18:1/26:1	0.8136110	0.8313211	0.8750525	0.9864140	0.2381388
LPI 18:1	0.9273928	0.7663751	0.9179075	0.9624464	0.2352996
LPS 16:0	0.9959272	0.9999702	0.9999702	0.7257249	0.0622278

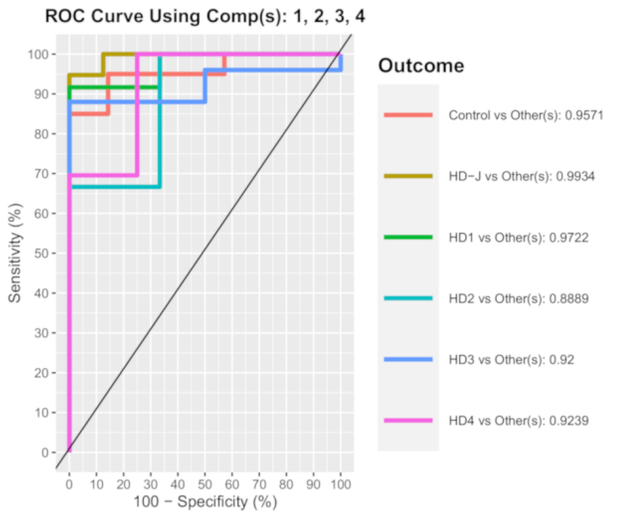

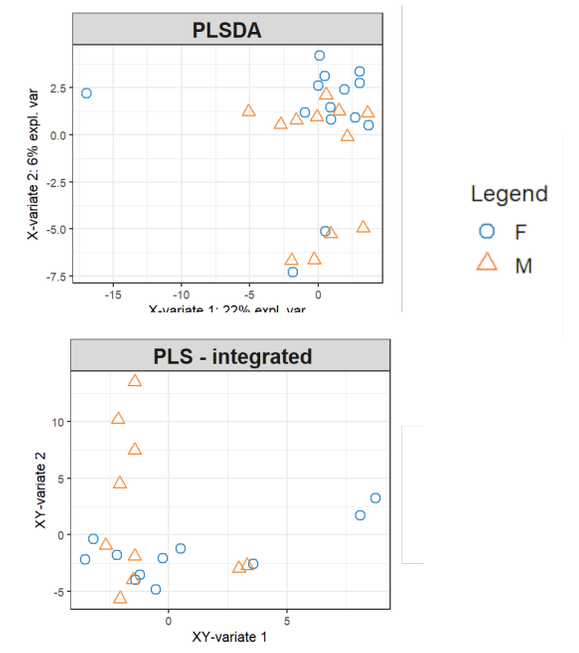

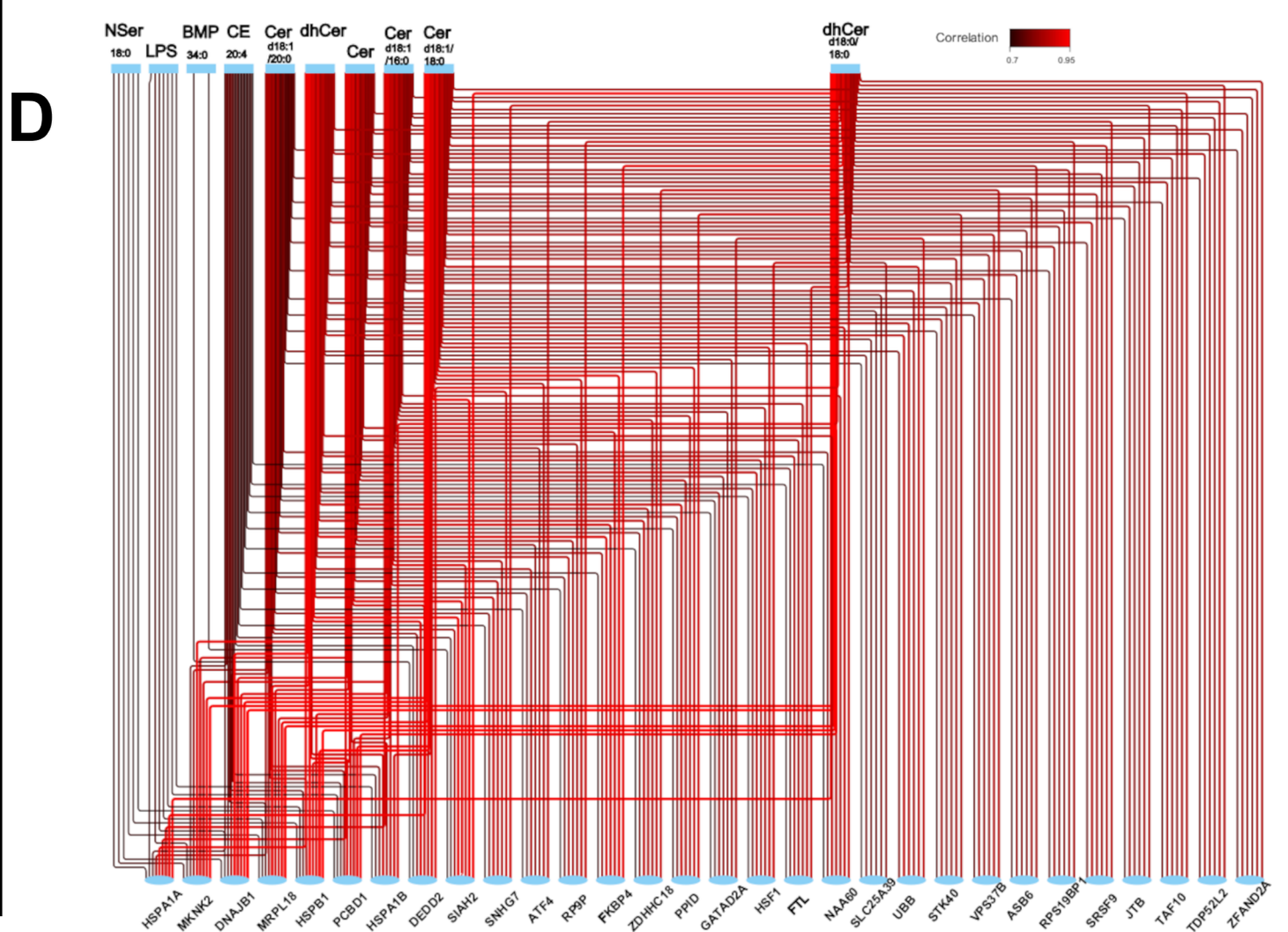

Figure S4. Increased CD44 expression in the Caudate of HD astrocytes. A) Immunofluorescent images depicting CD44 positive astrocytes (fibrous-like) (arrowhead) that are MT3 positive (arrow) in control and HD caudate nucleus. Scale Bar= 20 μm. **B**) Quantification of the percent of astrocytes in the Caudate that are CD44 positive using a two-tailed unpaired t-test. N=6 for control and 7 for HD. Data is shown as mean +/- SEM. P value= 0.0050. **C**) Quantification of the average process length of astrocytes in Control and HD measured by the length of GFAP positive processes using a two-tailed unpaired t-test. N=3 per condition, minimum of 12 cells per case. Data is shown as mean +/- SEM. P value= 0.0013. **D**) Quantification of the density of CD44 and MT3 positive astrocytes in the Caudate using a two-tailed unpaired t-test. N=6 for control and 7 for HD. Data is shown as mean +/- SEM. P value= 0.2548. **E**) Quantification of the density of CD44 negative (protoplasmic) and MT3 positive astrocytes in the Caudate using a two-tailed unpaired t-test. N=6 for control and 7 for HD. Data is shown as mean +/- SEM. P value= 0.0021. **F**) Immunohistochemical stain for CD44 in the caudate of control and HD samples. Note the labeling of pencil fibers and ventricle lining seen at the top of the image. The arrow indicates a CD44 positive cell in the caudate parenchyma not associated with large vessels or pencil fibers. Scale bar= 250μm. Insets – bottom row: Enlarged images of the regions shown in the black box showing the parenchymal CD44 positive cell in the top right corner of the HD image. Scale bar=100μm.

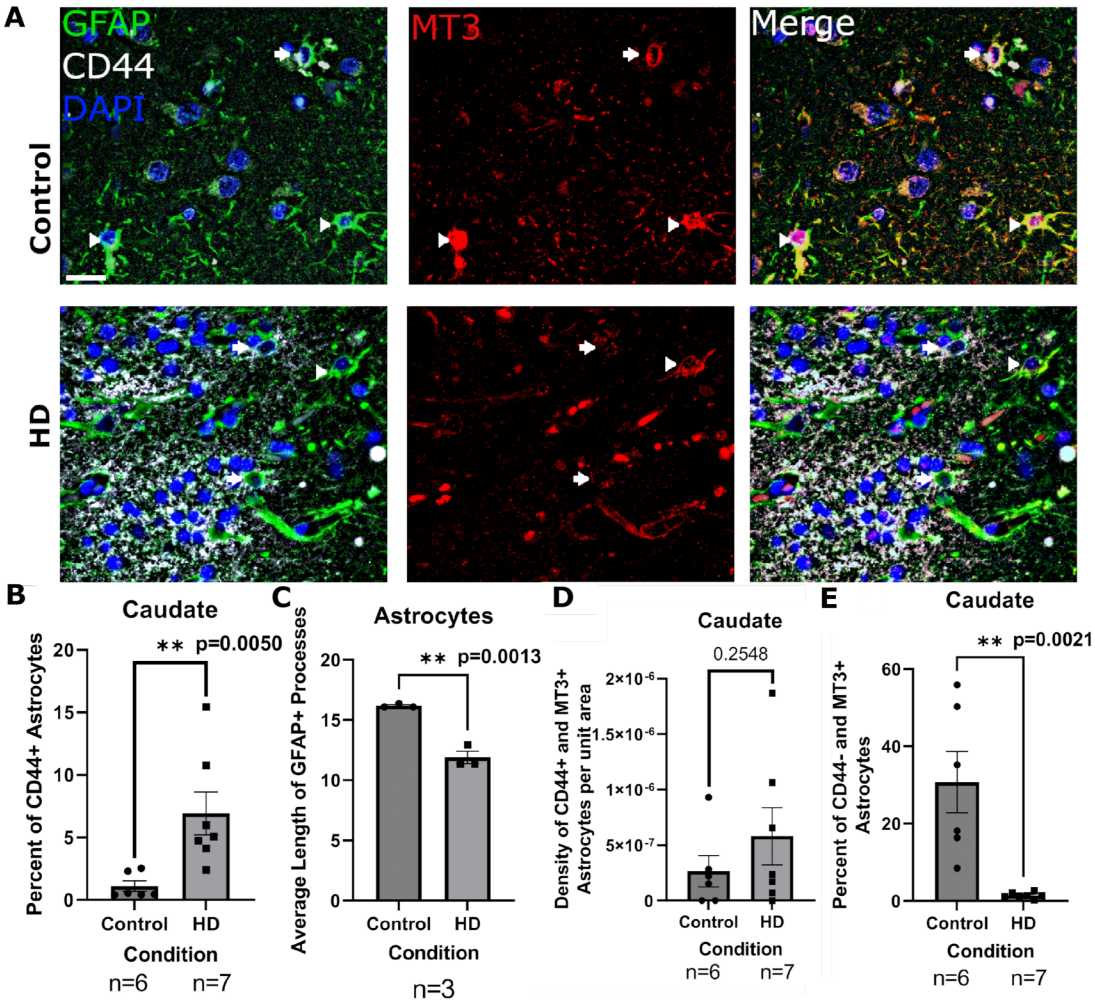
A
GFAP
CD44
DAPI
MT3
Merge
Control
HD
B
Caudate
** p=0.0050
Percent of CD44+ Astrocytes
Control
HD
Condition
n=6
n=7
C
Astrocytes
** p=0.0013
Average Length of GFAP+ Processes
Control
HD
Condition
n=3
D
Caudate
0.2548
Density of CD44+ and MT3+ Astrocytes per unit area
Control
HD
Condition
n=6
n=7
E
Caudate
** p=0.0021
Percent of CD44- and MT3+ Astrocytes
Control
HD
Condition
n=6
n=7

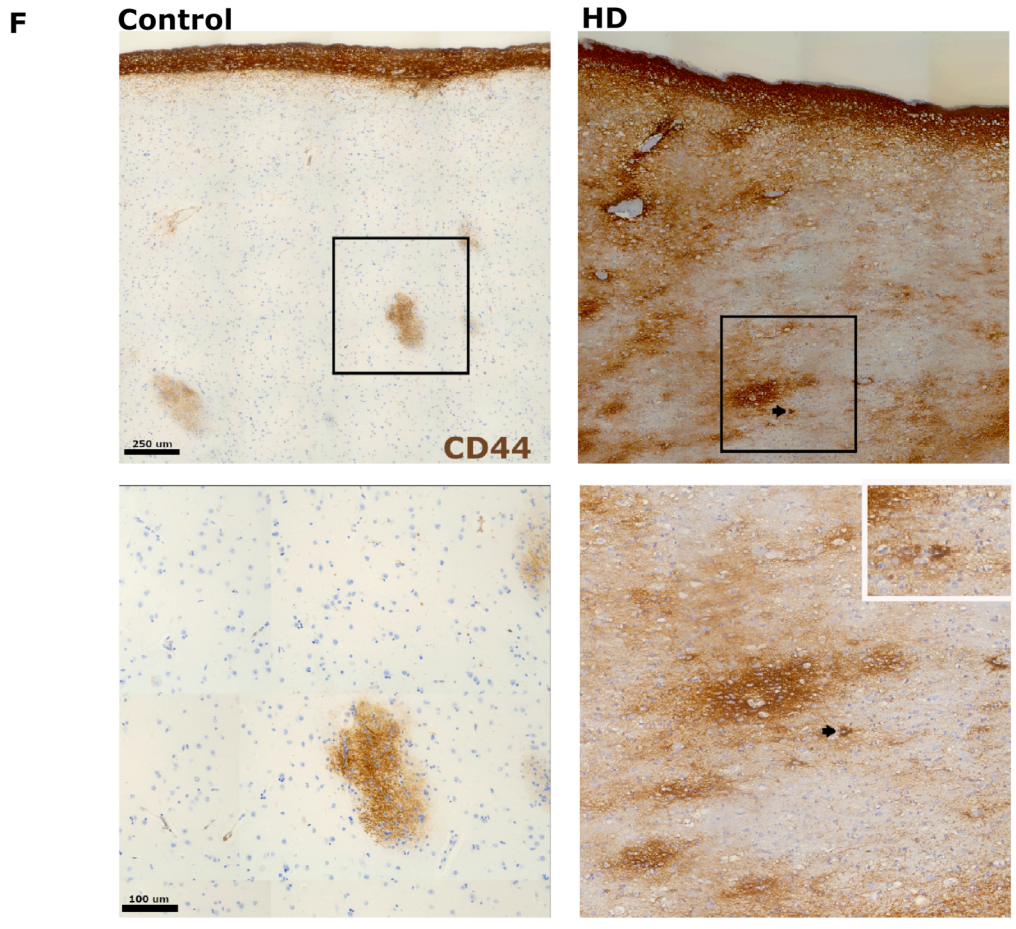
F
Control
HD
250 um
CD44
100 um

Figure S5. Astrocyte clusters and pseudotime analysis - related to Figure 3. A) t-SNE plots of all snRNAseq cells color-coded by donor (left), grade (middle), and sequencing batch (right). **B)** UMAP plots of all astrocytes split by condition (left - control and the right - HD), color-coded by clusters. **C)** Dot plot showing the expression of the top five cluster markers for the clusters in (**B**)**. D)** PHATE embeddings of all astrocytes with color-coded by pseudotime values in trajectory-1 (left) and trajectory-2 (right). High pseudotime values are shown in red, low in yellow. Arrows denote areas of high SLC1A2 expression (left) and high CD44 expression (right). The ridge plots (below) show frequency of grade (y axis) across pseudotime values (x axis). **E)** Heatmap showing gene ontology enrichment analysis for the genes that vary along pseudotime trajectories from high pseudotime values to low values as - shown in (D). The –log10 p value of enrichment of select pathways (y axis - rows) in each trajectory (x axis - columns) are coded by color. **F)** Barplots depicting the proportion of each protoplasmic (top) and each fibrous-like (bottom) astrocyte sub-cluster cells per donor. The plots are separated by control (left) and HD (right) donors. **G)** Barplots showing the proportion of each fibrous-like (top) and protoplasmic (bottom) astrocyte sub-cluster cells per HD grade/condition split by anatomic region (left – accumbens; center – caudate; right – cingulate).

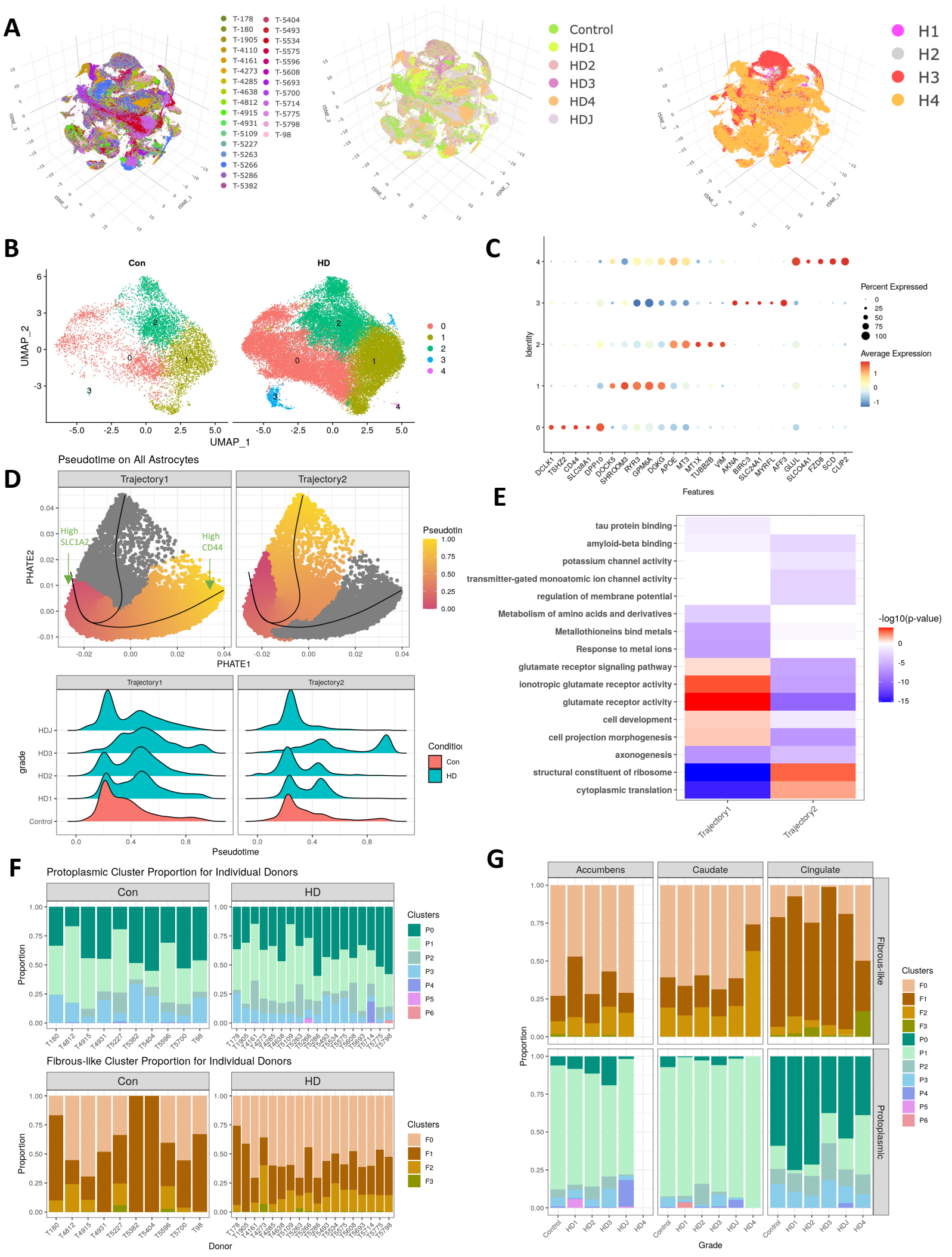
A
T-178
T-180
T-1905
T-4110
T-4161
T-4273
T-4285
T-4638
T-4812
T-4915
T-4931
T-5109
T-5227
T-5263
T-5266
T-5286
T-5382
T-5404
T-5493
T-5534
T-5575
T-5596
T-5608
T-5693
T-5700
T-5714
T-5775
T-5798
T-98
Control
HD1
HD2
HD3
HD4
HDJ
H1
H2
H3
H4
B
Con
HD
UMAP_2
UMAP_1
C
Percent Expressed
Average Expression
Identity
Features
DCLK1
TSHZ2
CD44
SLC38A1
DPP10
DOCK5
SHROOM3
RYR3
GPM6A
DGKG
APOE
MT3
MT1X
TUBB2B
VIM
AKNA
BIRC3
SLC24A1
MYRFL
AFF3
GLUL
SLCO4A1
FZD8
SCD
CLIP2
D
Pseudotime on All Astrocytes
Trajectory1
Trajectory2
High SLC1A2
High CD44
PHATE2
PHATE1
Pseudotim
grade
HDJ
HD3
HD2
HD1
Control
Pseudotime
Conditio
Con
HD
E
tau protein binding
amyloid-beta binding
potassium channel activity
transmitter-gated monoatomic ion channel activity
regulation of membrane potential
Metabolism of amino acids and derivatives
Metallothioneins bind metals
Response to metal ions
glutamate receptor signaling pathway
ionotropic glutamate receptor activity
glutamate receptor activity
cell development
cell projection morphogenesis
axonogenesis
structural constituent of ribosome
cytoplasmic translation
-log10(p-value)
Trajectory1
Trajectory2
F
Protoplasmic Cluster Proportion for Individual Donors
Con
HD
Proportion
Clusters
Fibrous-like Cluster Proportion for Individual Donors
Donor
G
Accumbens
Caudate
Cingulate
Fibrous-like
Protoplasmic
Proportion
Clusters
Grade
Control
HD1
HD2
HD3
HDJ
HD4

Figure S6. Differential gene expression in astrocyte clusters. A) Barplot depicting of the number of differential expressed genes increased (up) and decreased (down) in astrocyte sub-clusters comparing HD vs control. **B**) Heatmap showing GO, KEGG, and Reactome pathway enrichment analysis of the differentially expressed genes (DEGs) from (A) for each specified sub-cluster (columns). The colors indicate the –log10(p-value) of the enrichment score, with the red tiles showing terms enriched in DEGs increased in HD, and blue tiles showing terms enriched in DEGs decreased in HD. White tiles indicate no significance.

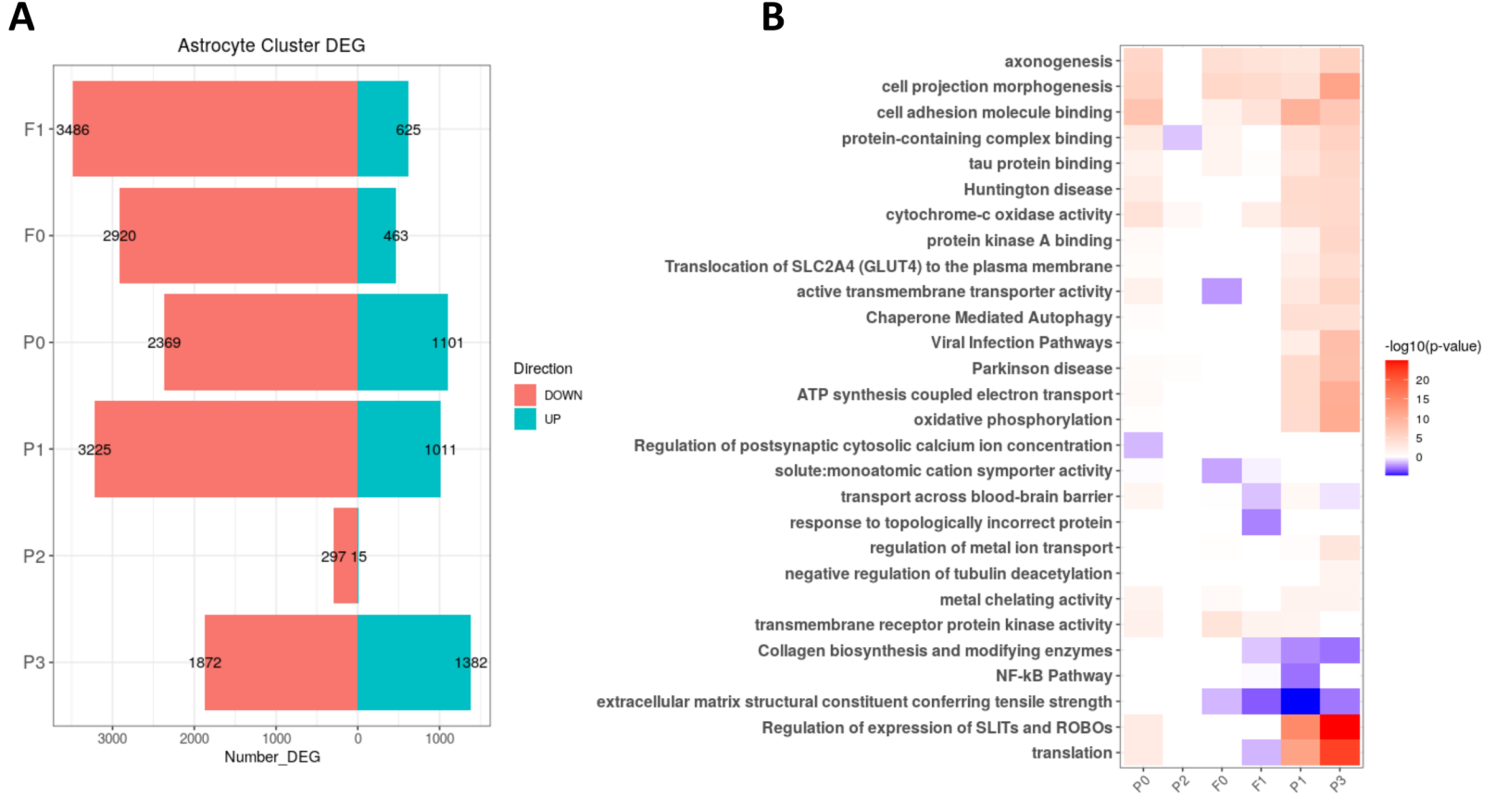
A
Astrocyte Cluster DEG
F1
F0
P0
P1
P2
P3
3486
625
2920
463
2369
1101
3225
1011
297
15
1872
1382
3000
2000
1000
0
1000
Number_DEG
Direction
DOWN
UP
B
axonogenesis
cell projection morphogenesis
cell adhesion molecule binding
protein-containing complex binding
tau protein binding
Huntington disease
cytochrome-c oxidase activity
protein kinase A binding
Translocation of SLC2A4 (GLUT4) to the plasma membrane
active transmembrane transporter activity
Chaperone Mediated Autophagy
Viral Infection Pathways
Parkinson disease
ATP synthesis coupled electron transport
oxidative phosphorylation
Regulation of postsynaptic cytosolic calcium ion concentration
solute:monoatomic cation symporter activity
transport across blood-brain barrier
response to topologically incorrect protein
regulation of metal ion transport
negative regulation of tubulin deacetylation
metal chelating activity
transmembrane receptor protein kinase activity
Collagen biosynthesis and modifying enzymes
NF-kB Pathway
extracellular matrix structural constituent conferring tensile strength
Regulation of expression of SLITs and ROBOs
translation
P0
P2
F0
F1
P1
P3
-log10(p-value)
20
15
10
5
0

Figure S7. Differential gene expression in HD neurons. **A**) Volcano plots of differentially expressed genes (DEGs) from accumbens, red indicates DEGs increased in HD, and blue indicates DEGs decreased in HD samples. dSPN (direct-pathway spiny projection neurons) DEGs – left, GABAergic neurons middle panel (A'), and iSPN (indirect-pathway SPNs) right panel (A''). **B**) Same analysis as (A) but for caudate neurons. **C**) Same as A but for cingulate GABAergic neurons (left panel) and Glut (Glutamatergic) neurons right panel - C'. D) Bar plot displaying the number of DEGs increased (up) and decreased (down) in HD for the major neuronal type across the three brain regions analyzed. Only the top 1000 genes with absolute log foldchange > 0.5 and adjusted p-value < 0.05 were considered. **E**) Heatmap displaying the -log10(p-value) of the GO terms (rows) enriched in DEGs comparing HD to control clusters (columns from A-C); red color indicates terms significantly enriched in DEGs increased in HD, and blue indicates terms significantly enriched in DEGs decreased in HD, and white means no significance. **F**) Representative images of immunohistochemical stain for LGR5 and (brown) with blue hematoxylin counter-stain to label nuclei in HD and control caudate nucleus tissue. Arrows indicate LGR5 positive neurons, while arrowheads depict indicate negative neurons. Scale bar = 50 μm. The barplot below shows the quantification of the proportion of caudate neurons that were LGR5 positive in HD vs controls. Unpaired one-tailed t-test with N=5 for control and HD. Data is shown as mean +/- SEM. p value= 0.0482.

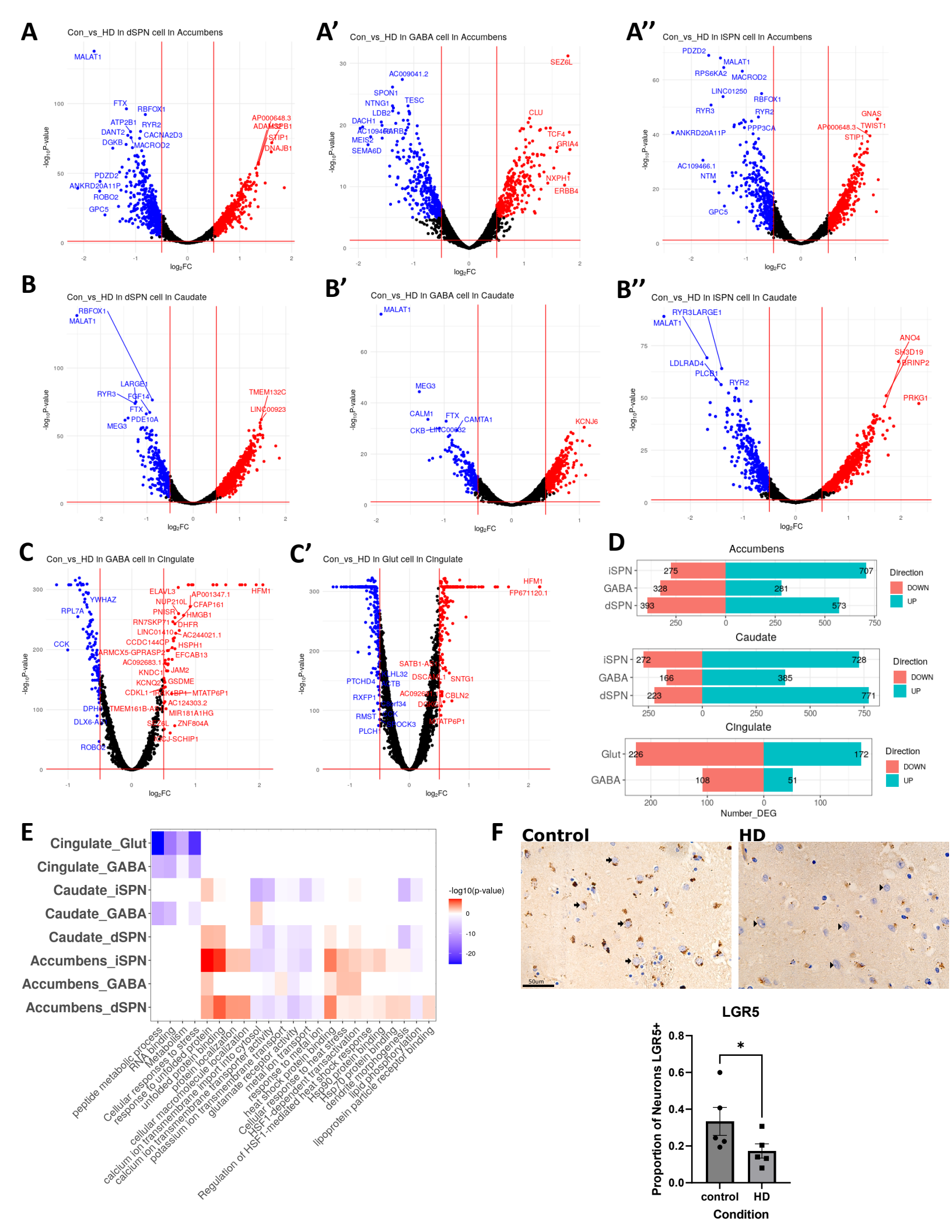
A
Con_vs_HD In dSPN cell In Accumbens
A'
Con_vs_HD In GABA cell In Accumbens
A''
Con_vs_HD In iSPN cell In Accumbens
B
Con_vs_HD In dSPN cell In Caudate
B'
Con_vs_HD In GABA cell In Caudate
B''
Con_vs_HD In iSPN cell In Caudate
C
Con_vs_HD In GABA cell In CIngulate
C'
Con_vs_HD In Glut cell In CIngulate
-log10P-value
log2FC
D
Accumbens
iSPN 275 707
GABA 328 281
dSPN 393 573
Caudate
iSPN 272 728
GABA 166 385
dSPN 223 771
CIngulate
Glut 226 172
GABA 108 51
Direction
DOWN
UP
Number_DEG
E
Cingulate_Glut
Cingulate_GABA
Caudate_iSPN
Caudate_GABA
Caudate_dSPN
Accumbens_iSPN
Accumbens_GABA
Accumbens_dSPN
-log10(p-value)
peptide metabolic process
RNA binding
Metabolism
Cellular responses to stress
response to unfolded protein
unfolded protein binding
protein localization
cellular macromolecule localization
calcium ion transmembrane import into cytosol
calcium ion transmembrane transporter activity
potassium ion transmembrane transport
glutamate receptor activity
metal ion transport
response to metal ion
heat shock protein binding
Cellular response to heat stress
HSF1-dependent transactivation
Regulation of HSF1-mediated heat shock response
Hsp90 protein binding
Hsp70 protein binding
dendrite morphogenesis
lipid phosphorylation
lipoprotein particle receptor binding
F
Control
HD
50um
LGR5
Proportion of Neurons LGR5+
control
HD
Condition
*

Figure S8. Decreased CLU expression in cingulate HD astrocytes. A) Representative multiplex immunofluorescence images of the cingulate cortex labeled for nuclei (DAPI-blue) and GFAP (green) to detect astrocytes (left), and CLU (red-middle). A merge of the three channels is shown on the right. Arrows indicate DAPI, GFAP and CLU positive cells (CLU positive astrocytes) and arrowheads indicate CLU negative astrocytes. Scale bar=20μm. **B**) Quantification of the percent of CLU positive astrocytes in the Cingulate. Unpaired two-tailed t-test with N=8 for control and 5 for HD. Data is shown as mean +/- SEM. P value= 0.0173. **C**) Same as A but for the caudate. **D**) Quantification of the percent of CLU positive astrocytes in the Caudate. Unpaired two-tailed t-test used with N=10 for control and 5 for HD. Data is shown as mean +/- SEM. P value= 0.6259.

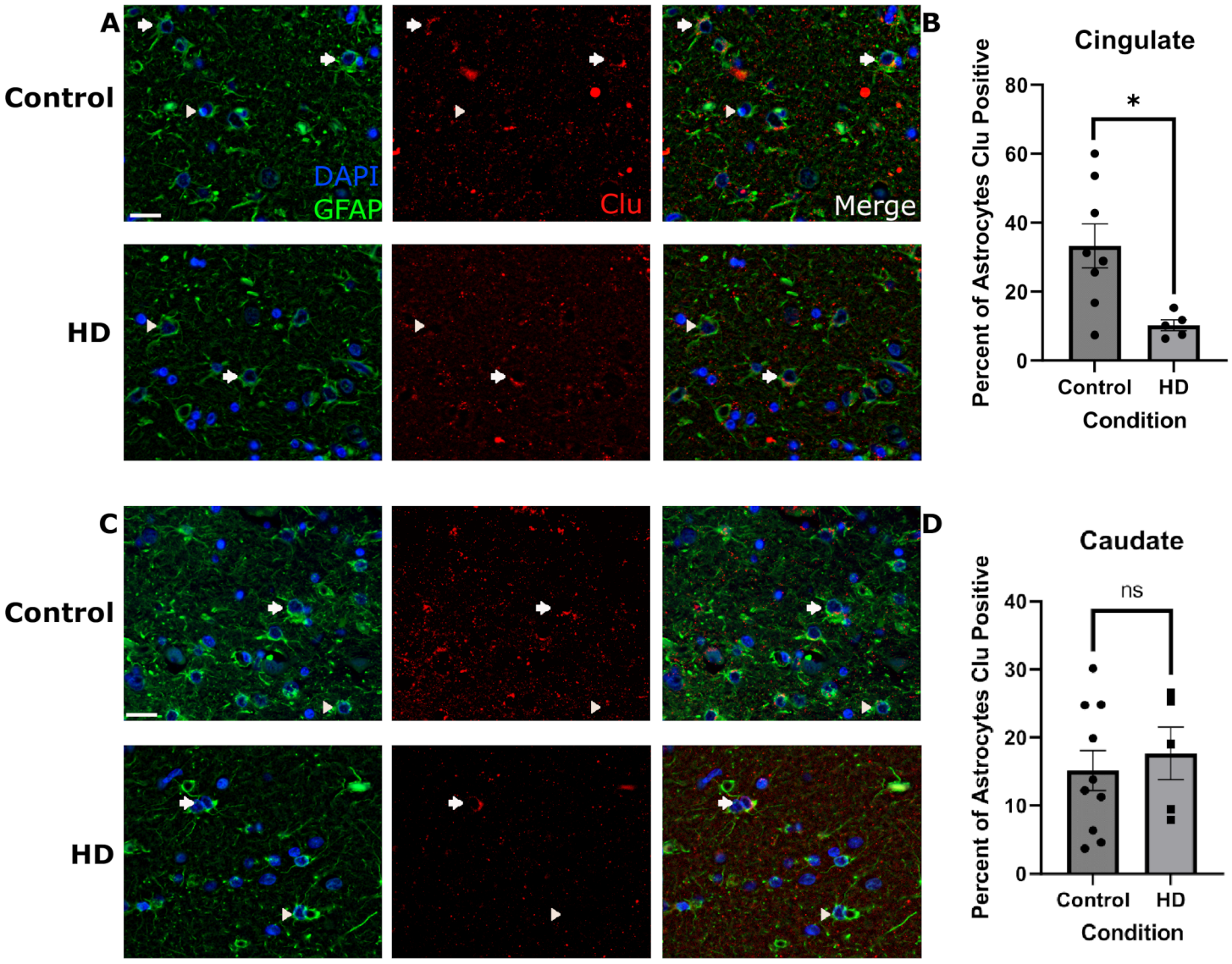
A
B
Control
HD
DAPI
GFAP
Clu
Merge
Cingulate
Percent of Astrocytes Clu Positive
80
60
40
20
0
*
Control
HD
Condition
C
D
Control
HD
Caudate
Percent of Astrocytes Clu Positive
40
30
20
10
0
ns
Control
HD
Condition

Figure S9. Astrocyte gene expression in vitro and in sub-clusters. Related to figure 7. A) Gene expression quantification (real-time quantitative PCR) of MT3 and other metallothioneins in MT3 overexpressing versus GFP control astrocytes. The gene expression was normalized for GAPDH control. The delta-delta CT's were log-normalized. One sample t-test one-tailed test. P-value of 0.0125 for *MT3* and non-significant for other metallothioneins. **B-C**) Quantification of select MT family genes (B) and *CLU* (C) in CLU overexpressing astrocytes, The data is normalized and shown as per A. One sample two-tailed t-test, p-value= 0.1681 for MT1E and 0.2777 for MT1A, and p-value= 0.0016 for CLU in C. **D**) Real-time qPCR gene expression quantification of SLC1A2 and GLUL in MT3 overexpressing astrocytes normalized by GAPDH and the delta-delta CT's were compared with a one-tailed one-sample t-test. MT3 overexpressing astrocytes significantly increased expression of *GLUL* (p=0.0352) and *SLC1A2* (p=0.0497). n = 3 biological replicates for A-D. **E-F**) Violin plots showing the normalized expression of *MT2A, MT3, MT1E*, and, *MT1G* for fibrous-like and protoplasmic astrocyte sub-clusters by region and condition. **G**) Top two panels show violin plots of *GLUL* and *SLC1A2* in protoplasmic astrocytes with high MT3 vs low MT3 (top panels). Cells with normalized MT3 expression > 2 were considered MT3-high. p-values are indicated - as calculated using a Wilcox test. Bottom two panels show dotplots of normalized expression of MT3 and *GLUL* (left) and *SLC1A2* (right), respectively. Line of best fit (blue) and p values as calculated using cor.test are indicated. See main text for correlation coefficients.

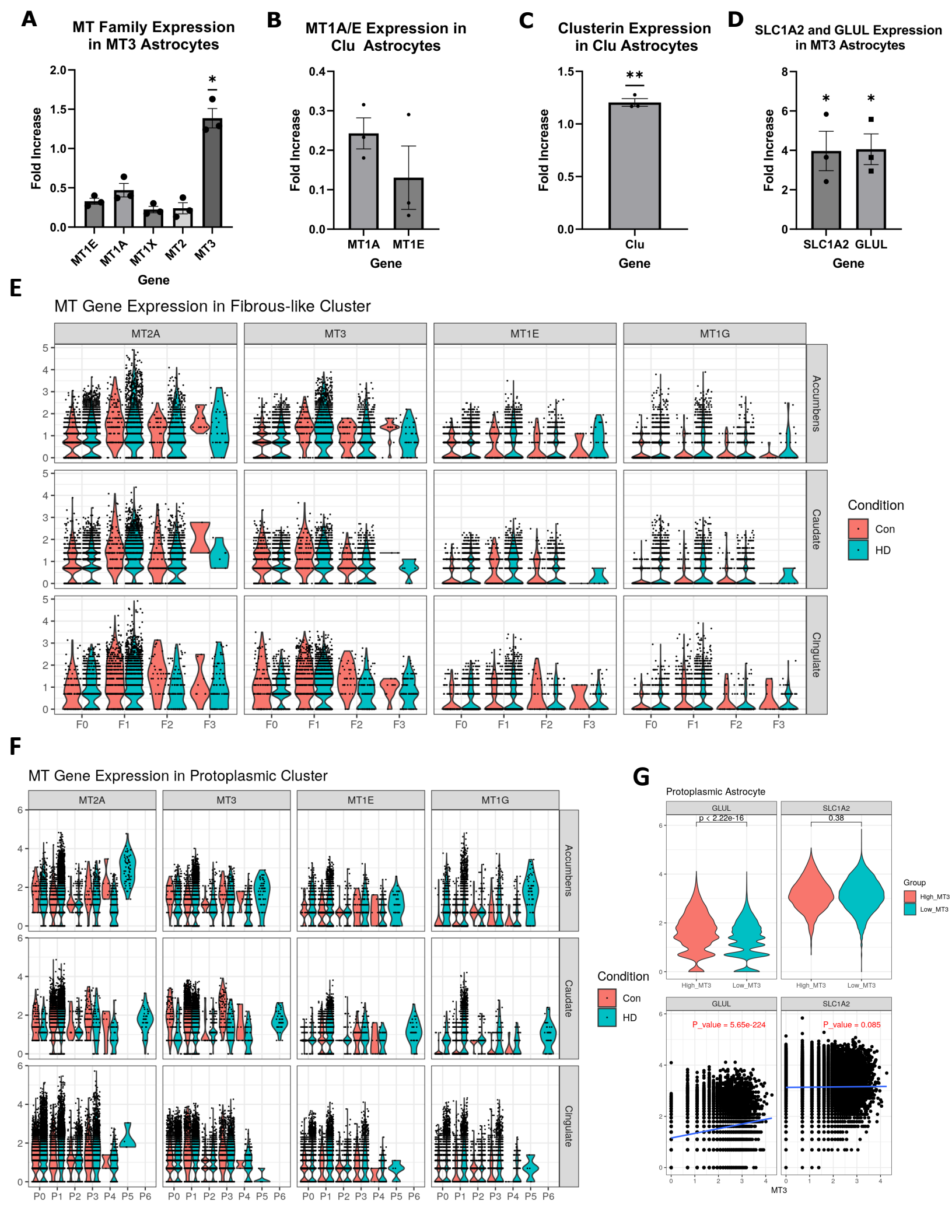
A
MT Family Expression in MT3 Astrocytes
Fold Increase
Gene
MT1E
MT1A
MT1X
MT2
MT3
B
MT1A/E Expression in Clu Astrocytes
C
Clusterin Expression in Clu Astrocytes
Clu
D
SLC1A2 and GLUL Expression in MT3 Astrocytes
SLC1A2
GLUL
E
MT Gene Expression in Fibrous-like Cluster
MT2A
MT3
MT1E
MT1G
Accumbens
Caudate
Cingulate
F0
F1
F2
F3
Condition
Con
HD
F
MT Gene Expression in Protoplasmic Cluster
P0
P1
P2
P3
P4
P5
P6
G
Protoplasmic Astrocyte
p < 2.22e-16
0.38
High_MT3
Low_MT3
Group
P_value = 5.65e-224
P_value = 0.085
MT3

Figure S10. snRNAseq of myeloid population in HD and control brains. **A**) UMAP plot displaying the main myeloid lineages. Three cell types are indicated: microglia, T-cell, and monocytes. **B**) Dot plot showcasing markers for the three cell types. **C**) Volcano plot of genes that are differentially expressed in HD for microglia in the accumbens (red highlight = genes significantly higher in HD samples, blue highlight = genes significantly lower in HD samples). **D**) Same as (C) but for microglia in the cingulate. **E**) Same as (C) but for microglia in the caudate. **F**) Heatmap showing the log10(p-value) of the GO terms enriched in the DEGs from (C), (D), and (E). The red tiles show terms enriched in DEGs increased in HD and blue tiles show terms enriched in DEGs decreased in HD. White tiles indicate no significance.

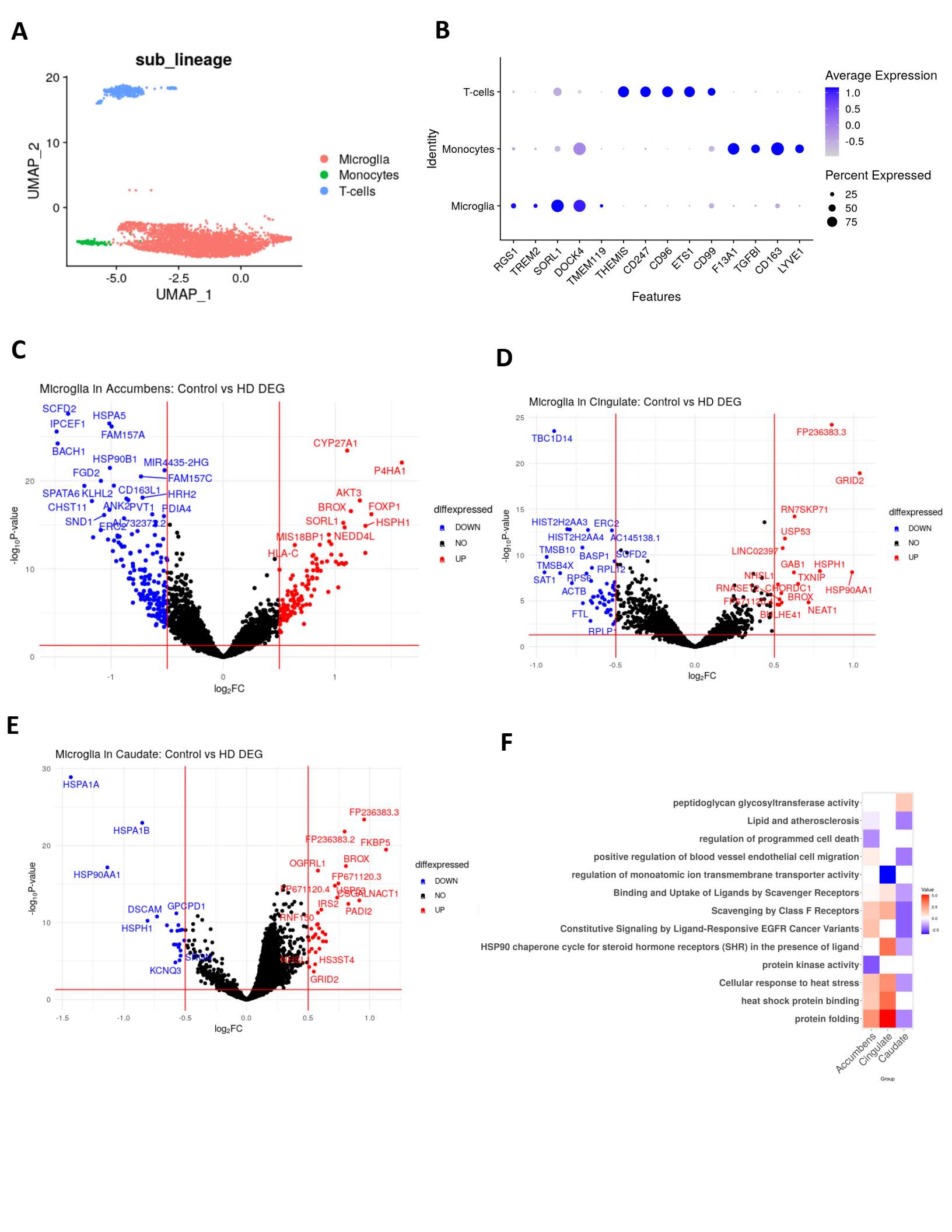
A
sub_lineage
UMAP_2
UMAP_1
Microglia
Monocytes
T-cells
B
Identity
T-cells
Monocytes
Microglia
Features
RGS1
TREM2
SORL1
DOCK4
TMEM119
THEMIS
CD247
CD96
ETS1
CD99
F13A1
TGFBI
CD163
LYVE1
Average Expression
Percent Expressed
C
Microglia In Accumbens: Control vs HD DEG
-log10P-value
log2FC
diffexpressed
DOWN
NO
UP
D
Microglia In Cingulate: Control vs HD DEG
E
Microglia In Caudate: Control vs HD DEG
F
peptidoglycan glycosyltransferase activity
Lipid and atherosclerosis
regulation of programmed cell death
positive regulation of blood vessel endothelial cell migration
regulation of monoatomic ion transmembrane transporter activity
Binding and Uptake of Ligands by Scavenger Receptors
Scavenging by Class F Receptors
Constitutive Signaling by Ligand-Responsive EGFR Cancer Variants
HSP90 chaperone cycle for steroid hormone receptors (SHR) in the presence of ligand
protein kinase activity
Cellular response to heat stress
heat shock protein binding
protein folding
Accumbens
Cingulate
Caudate
Group
Value

Figure S11. MT3 astrocytes modulate microglial function. A) Cartoon depicting the trans-well co-culture experiment between astrocytes and microglia (HMC3 cells). **B**) PCA plot of the first two component of the bulk-RNAseq samples: control samples are HMC3's co-cultured with GFP astrocytes or untransduced astrocytes. Experimental conditions are HMC3's co-cultured with CLU or MT3 overexpressing astrocytes. Mono-cultures of microglial cells are also shown. Note that co-culture is a major driver of gene expression variation. **C-D**) Volcano plots showing log-fold change of gene expression and adjusted p values when comparing control (HA/GFP = human astrocytes or GFP transduced astrocyte control group co-cultures) versus microglia co-cultured with CLU astrocytes (C) or MT3-overexpressing astrocytes. **E**) Heatmap showing the GO enrichment analysis of DEGs from D. The log10(p-value) of enrichment score is shown. Red tiles showing GO enriched in DEGs increased, and blue indicates GO terms enriched in DEGs decreased in HMC's co-cultured with MT3 astrocytes versus control astrocytes. **F**) Pre-ranked geneset enrichment analysis measuring the enrichment of DEG's from (D), CAG-correlated gene sets from Figure 1E, and the GO for phagocytosis, in the ranked DEG from Figure S10C-E and ranked cluster 0 markers (cluster 0 = microglial cluster from Figure S10A). The adjusted p values and normalized enrichment scores (NES) are indicated. Red stars indicate significance. **G**) Bar plot showing the percentage of microglia (HMC's) with phagocytosed GFP-labeled beads. The conditions indicated are: GFP = Microglia in co-culture with GFP astrocytes, CLU = Microglia in co-culture with CLU astrocytes, MT3 = Microglia in co-culture with MT3 astrocytes). N = 4 biological replicates. Paired two-tailed t-tests. The p values are indicated.

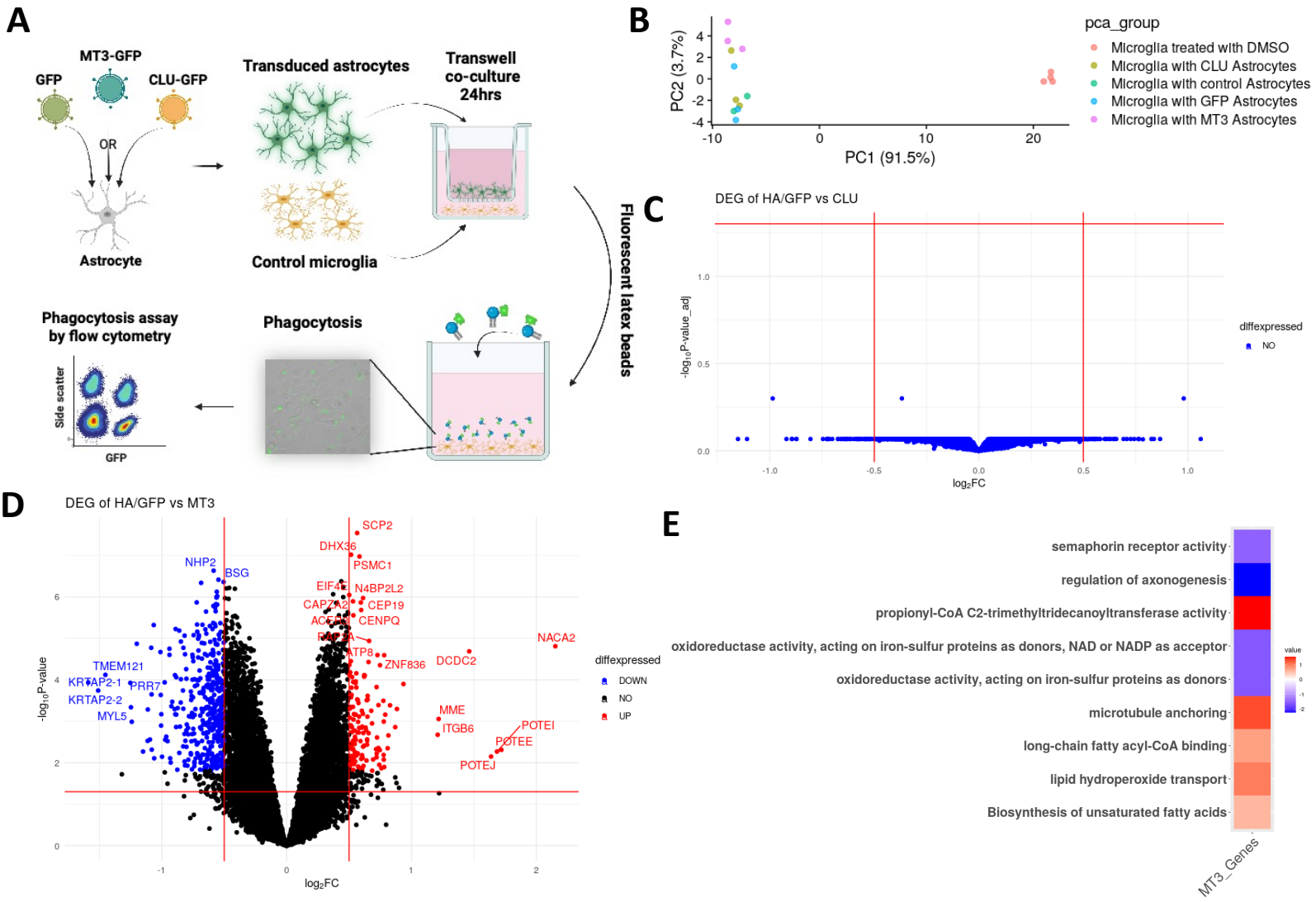

F

Accumbens DEG

	Pathway	Gene ranks	NES	pval	padj
	MT3 DEG UP		1.45	$2.4 \cdot 10^{-2}$	$6.1 \cdot 10^{-2}$
	MT3 DEG DOWN		0.65	$9.9 \cdot 10^{-1}$	$9.9 \cdot 10^{-1}$
*	Increased CAG		-1.36	$3.0 \cdot 10^{-3}$	$1.5 \cdot 10^{-2}$
	Decreased CAG		0.70	$9.9 \cdot 10^{-1}$	$9.9 \cdot 10^{-1}$
	Phagocytosis_GO:0006909		-1.21	$1.9 \cdot 10^{-1}$	$3.2 \cdot 10^{-1}$

0 2000 4000 6000

Cingulate DEG

	Pathway	Gene ranks	NES	pval	padj
*	MT3 DEG UP		1.66	$4.5 \cdot 10^{-3}$	$2.2 \cdot 10^{-2}$
	MT3 DEG DOWN		-0.97	$5.1 \cdot 10^{-1}$	$9.3 \cdot 10^{-1}$
	Increased CAG		-0.80	$9.3 \cdot 10^{-1}$	$9.3 \cdot 10^{-1}$
	Decreased CAG		-0.74	$9.3 \cdot 10^{-1}$	$9.3 \cdot 10^{-1}$
	Phagocytosis_GO:0006909		-0.94	$5.7 \cdot 10^{-1}$	$9.3 \cdot 10^{-1}$

0 1000 2000 3000 4000 5000

Caudate DEG

	Pathway	Gene ranks	NES	pval	padj
	MT3 DEG UP		1.15	$2.4 \cdot 10^{-1}$	$3.0 \cdot 10^{-1}$
	MT3 DEG DOWN		1.31	$7.8 \cdot 10^{-2}$	$2.9 \cdot 10^{-1}$
	Increased CAG		1.14	$1.2 \cdot 10^{-1}$	$2.9 \cdot 10^{-1}$
	Decreased CAG		0.70	$9.4 \cdot 10^{-1}$	$9.4 \cdot 10^{-1}$
	Phagocytosis_GO:0006909		1.20	$2.2 \cdot 10^{-1}$	$3.0 \cdot 10^{-1}$

0 2000 4000 6000 8000

Cluster 0 markers

	Pathway	Gene ranks	NES	pval	padj
	MT3 DEG UP		0.82	$7.7 \cdot 10^{-1}$	$7.7 \cdot 10^{-1}$
	MT3 DEG DOWN		1.33	$1.2 \cdot 10^{-1}$	$2.0 \cdot 10^{-1}$
	Increased CAG		1.44	$1.7 \cdot 10^{-2}$	$4.2 \cdot 10^{-2}$
	Decreased CAG		1.23	$2.1 \cdot 10^{-1}$	$2.6 \cdot 10^{-1}$
*	Phagocytosis_GO:0006909		2.26	$5.2 \cdot 10^{-4}$	$2.6 \cdot 10^{-3}$

0 500 1000 1500 2000 2500

G

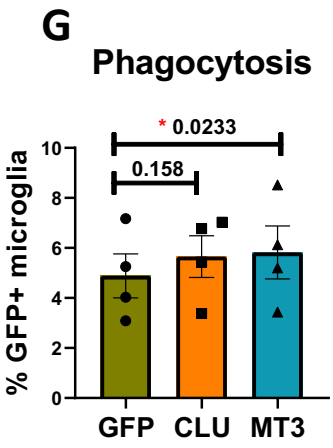

Supplementary References

1. Runne, H. et al. Dysregulation of gene expression in primary neuron models of Huntington's disease shows that polyglutamine-related effects on the striatal transcriptome may not be dependent on brain circuitry. The Journal of neuroscience : the official journal of the Society for Neuroscience 28, 9723-9731 (2008).

2. Niccolini, F. et al. Altered PDE10A expression detectable early before symptomatic onset in Huntington's disease. Brain 138, 3016-3029 (2015).

3. Malaiya, S. et al. Single-Nucleus RNA-Seq Reveals Dysregulation of Striatal Cell Identity Due to Huntington's Disease Mutations. The Journal of neuroscience : the official journal of the Society for Neuroscience 41, 5534-5552 (2021).

4. Lee, H. et al. Cell Type-Specific Transcriptomics Reveals that Mutant Huntingtin Leads to Mitochondrial RNA Release and Neuronal Innate Immune Activation. Neuron (2020).

5. Matejuk, A. & Ransohoff, R.M. Crosstalk Between Astrocytes and Microglia: An Overview. Front Immunol 11, 1416 (2020).

6. Thrupp, N. et al. Single-Nucleus RNA-Seq Is Not Suitable for Detection of Microglial Activation Genes in Humans. Cell reports 32, 108189 (2020).

7. Taban, Q., Mumtaz, P.T., Masoodi, K.Z., Haq, E. & Ahmad, S.M. Scavenger receptors in host defense: from functional aspects to mode of action. Cell Commun Signal 20, 2 (2022).

8. Al-Dalahmah, O. et al. Re-convolving the compositional landscape of primary and recurrent glioblastoma reveals prognostic and targetable tissue states. Nature communications 14, 2586 (2023).